



Effect of Excess Silicon and Small Copper Content on Intergranular Corrosion of 6000-Series Aluminum Alloys

Magnus Hurlen Larsen,^{a,*} John Charles Walmsley,^{b,c} Otto Lunder,^{c,**}
and Kemal Nisancioglu^{a,*,*,z}

^aDepartment of Materials Science and Engineering and ^bDepartment of Physics, Norwegian University of Science and Technology, N-7491 Trondheim, Norway
^cSINTEF Materials and Chemistry, N-7465 Trondheim, Norway

The required strength and ductility of heat-treatable AlMgSi (6000-series) alloys are often obtained by alloying with either a small amount of Cu or a large excess of Si compared to the stoichiometric Mg/Si ratio corresponding to the Mg₂Si phase. Both approaches may cause susceptibility to intergranular corrosion (IGC) as a result of unfavorable heat-treatment. Whether alloying with Cu or excess Si gives the optimal combination of mechanical properties and IGC resistance is a controversial subject. The corrosion behavior of a model alloy containing 0.2% Cu is compared with an essentially Cu-free alloy with an excess Si/Mg composition ratio (i.e., unbalanced) by using accelerated corrosion tests and electron optical characterization. In general, the Cu-containing alloy showed a higher susceptibility to IGC than the Cu-free, excess Si alloy. The Cu-containing alloy was especially susceptible in the underaged condition. The Cu-free, excess Si alloy became completely resistant to IGC by removing the cathodic intermetallic particles from the surface by selective etching or by purging the dissolved oxygen from the solution, whereas the Cu-containing alloy was still susceptible to IGC after the same treatment. The difference in IGC susceptibility between the two alloys was attributed to the presence of a cathodic Cu-rich film and discrete Cu-containing particles along the grain boundaries of the Cu-containing alloy, while the cathodic sites on the unbalanced variant were restricted to the material surface. In addition, the IGC susceptibility of both alloys depended on the presence of solute (Si and Cu)-depleted zones adjacent to the grain boundaries.

© 2009 The Electrochemical Society. [DOI: 10.1149/1.3261804] All rights reserved.

Manuscript submitted August 14, 2009; revised manuscript received October 12, 2009. Published December 7, 2009.

The significance of copper content on the intergranular corrosion (IGC) of 6000-series aluminum alloys has been discussed for more than 60 years. The European skepticism of alloying aluminum with Cu and the preference of using excess amount of Si up to 1%, relative to the stoichiometric Mg/Si ratio for precipitation of the Mg₂Si phase (unbalanced alloys), can be traced back to Hug,¹ while the North American preference of using balanced alloys (stoichiometric content of Mg/Si ratio for Mg₂Si precipitation) with up to 0.4% Cu content, to achieve the same level of strength, ductility, and corrosion resistance, is articulated by Johnson and Wright.² Although the former paper elaborated the dangers of using as low as 0.1% Cu, the latter paper demonstrated increased IGC susceptibility associated with high Si content and advantages of using up to 0.4% Cu in the balanced material without the danger of IGC and with increased resistance to pitting corrosion.

With only a few exceptions,^{3,4} IGC of AlMgSi(Cu) alloys has been attributed to depletion of Si and/or Cu along grain boundaries,⁵⁻¹³ although no convincing experimental verification of this hypothesis has been provided. Solute depletion was expected to form a continuous anodic path along the grain boundaries. The significance of grain body and grain boundary precipitates as local cathodes in forming microgalvanic cells, which promote localized corrosion, has been discussed.⁵⁻¹⁴ However, there is little agreement about the nature and actual location of the phases that cause IGC. Precipitated elemental Si on grain boundaries was claimed to act as local cathodic sites in alloys containing excess Si, although there is substantial evidence to suggest that Si is an ineffective cathode in aluminum alloys.¹⁵⁻¹⁷

Earlier studies also emphasized the effect of composition, especially the effect of alloying elements, such as Mn and Cr, on the influence of Cu and/or Si.¹⁸⁻²³ The alloys were usually investigated in the artificially aged, peak strength, T6 condition. Comparing the effects of Cu and excess Si content based on the literature data is complicated by the significant variation in alloy composition, the varied thermomechanical history of their casting, fabrication routes, and the corrosion test methods used.

Our own recent work²⁴⁻²⁷ did not show any adverse effect of moderate Si excess on IGC susceptibility, and it was suggested that the effects reported earlier of excess Si in AlMgSi alloys must have rather been a result of the added presence of Cu. The grain boundary nanostructure of Cu-containing alloys was studied extensively, revealing the presence of a thin Cu-rich film along the grain boundaries of the susceptible underaged temper. The film was not present as a distinct crystallographic phase and was only made visible by energy-dispersive spectroscopy (EDS) X-ray mapping, which gave an upper limit to its thickness of a few nanometers. The IGC susceptibility was eliminated by artificial aging to the T6 temper, which transformed the film into discrete, Cu-containing particles. This result explained how Cu-containing 6000-series alloys could be made IGC-resistant by aging to the T6 temper, i.e., providing the fortunate coincidence of obtaining both the maximum strength and IGC resistance. It was shown further²⁸ that alloys with Si/Mg ratios of up to about 1.6 suffered only minor superficial localized corrosion, whereas the addition of only about 0.2% Cu to the same alloys introduced severe IGC susceptibility in the underaged temper.

The purpose of this work is to clarify whether the excess Si or presence of Cu is more harmful in terms of IGC susceptibility by accelerated corrosion testing, by evaluation of corrosion morphology, and by study of the grain boundary nanostructure of model alloys by transmission electron microscopy (TEM). The TEM work particularly focuses on the Cu-free model alloy with excess Si. Similar work on Cu-containing model alloys was published earlier.²⁴⁻²⁸

Experimental

Test materials.— The chemical compositions of the model alloys are given in Table I. Alloy A had a moderate excess of silicon compared to the stoichiometric Mg/Si ratio and a moderate Cu content (0.18 wt %). Alloy B was essentially Cu-free (0.004 wt %), but had a high excess of Si. Alloy A was extruded in an 8 MN laboratory press. Alloy B was supplied as a rolled plate with a thickness of 2 mm.

Both alloys were given the same solution heat-treatment for 30 min at 540°C, followed by water quenching or air cooling. After storage at room temperature for 4 h, both the air-cooled and water-cooled materials were artificially aged in an oil bath at 185°C for 42 min, 5 h, or 24 h to obtain the underaged, peak-aged (T6), and

* Electrochemical Society Student Member.

** Electrochemical Society Active Member.

^z E-mail: kemaln@material.ntnu.no

Table I. Chemical composition of the alloys used. The compositions were determined by using optical emission spectroscopy. All values except Mg/Si ratio are in weight percent.

	Si	Mg	Cu	Fe	Mn	Al	Mg/Si
Alloy A	0.60	0.52	0.18	0.21	0.14	Balance	0.87
Alloy B	1.31	0.40	0.004	0.33	0.08	Balance	0.31

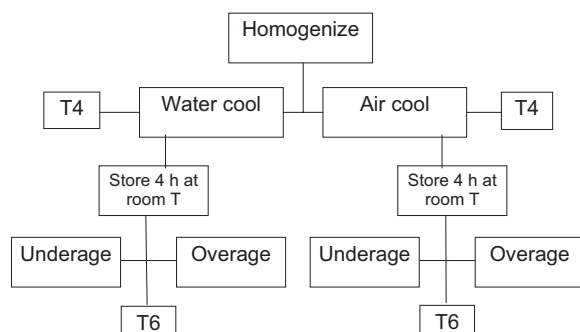
overaged conditions, respectively. Thus, the identification of the samples with respect to artificial aging followed the usual industrial norms, although the air-cooled material was slightly underaged at the outset. Whether the sample was air-cooled or water-cooled after homogenization is specified in the following text and figure captions. In addition, the solution heat-treated samples, which were subsequently air-cooled or water-cooled, were stored at an ambient temperature for at least 2 weeks without further heat-treatment to obtain their naturally aged conditions. For both air-cooled and water-quenched samples, this condition is referred to as the T4 temper in this paper with due reference to the different cooling procedures.

Table II gives a summarizing flow sheet for heat-treatment of Alloys A and B. This paper showed detailed results for Alloy B in all heat-treatment conditions shown in the table, while explicit results for Alloy A were limited to the water-quenched T4 condition. Comparisons of Alloy B with Alloy A in all the other tempers were confined to the text with reference to the comprehensive earlier work on Alloy A.²⁴⁻²⁸

Recent work with alloys of Type A, comparing directly the identical heat-treatment procedures relevant to the present paper (solution heat-treatment followed by water quenching or air cooling, followed by artificial aging or storing in the laboratory), indicated that the composition and temper were more important for IGC than whether the samples were extruded or rolled during fabrication.²⁹

Characterization of microstructure.— Plan view samples for scanning electron microscopy (SEM) were prepared by mechanical grinding and polishing to a 1 μm diamond paste finish. The samples were then electropolished for 2 min at an applied voltage of 12 V in a solution consisting of 1 part of HNO_3 and 2 parts of CH_3OH by volume, maintained at -32 to -37°C . The electropolishing step enhanced the visibility of the grain boundaries and grain boundary precipitates. It also altered the chemical composition of the grain boundary precipitates by preferential dissolution, thereby rendering quantitative analysis difficult in this surface condition.²⁴

Samples for TEM were prepared by mechanical thinning of samples to a thickness below 100 μm . Foil disks (3 mm diameter) were punched out and electropolished until perforation occurred in the electropolishing bath specified above. Before the TEM analysis, the foils were ion-beam-milled at a low angle for final thinning and removal of surface contamination.

Table II. Overall summary of heat-treatment procedures used for Alloys A and B.

The TEM work was performed on a JEOL2010F field-emission transmission electron microscope (FETEM) operated in the scanning mode at an accelerating voltage of 200 kV. Care was taken to align the grain boundaries parallel to the incident electron beam. Element map acquisition times were 1–3 h, depending on the foil thickness and mapping area. The element maps were further processed to produce composition profiles as a function of distance from the grain boundary using a software routine described in detail elsewhere.²⁸

Corrosion testing.— Before the IGC test, the samples were degreased in ethanol and acetone, etched for 3 min in 7.5 wt % NaOH at 55 – 60°C , rinsed in distilled water, desmutted for 2 min in concentrated HNO_3 , and rinsed again, as defined in the test standard. The alkaline etch removed the electrochemically active, nanocrystalline surface layer present on rolled surfaces.³⁰⁻³² Some samples were further pretreated for 30 s in fluoronitric acid (0.4 vol % HF + 35% HNO_3) at room temperature to etch intermetallic particles from the surface.^{33,34}

The accelerated IGC test procedure described in the British Standard BS ISO 11846 B³⁵ was used to investigate the corrosion performance of the materials. The test involved a 24 h immersion in an acidified salt solution (3 wt % NaCl + 1 vol % HCl). The mode and severity of corrosion attack were assessed by investigation of metallographic cross sections. Similar testing was also performed on selected specimens by using the same solution from which dissolved oxygen was removed by bubbling pure nitrogen.

Electrochemical testing.— Electrochemical measurements were performed using a Gill AC potentiostat and a saturated calomel electrode (SCE) reference. All potentials reported herein were with reference to SCE. The experiments were performed in either neutral 3% NaCl or acidified (by 1 vol % HCl) 3% NaCl solution. The solution was exposed to ambient laboratory atmosphere. The temperature was maintained at 25°C . For electrochemical characterization of Si, a piece of solar grade and high purity silicon with electrical contact was embedded in an epoxy resin. A Cu electrode was also prepared from an electrical grade and a high purity Cu plate. The sample was mounted in a polytetrafluoroethylene sample holder, providing an exposed circular area of 1.33 cm^2 with electrical contact to the back of the specimen. Both samples were metallographically ground and polished to 1 μm diamond finish using ethanol as lubricant. They were then ultrasonically cleaned in acetone, dried, and immediately transferred to the test cell.

Results

SEM.— The water-quenched Cu-containing alloy (Alloy A) in the underaged temper and a similar alloy, which was air-cooled after extrusion, have been studied earlier.^{25,27,28} The unbalanced Alloy B was therefore characterized in similar conditions for comparison with the corresponding tempers of the Cu-containing alloy.

The solution heat-treated and slowly air-cooled Alloy B had extensive grain boundary precipitation, as shown in Fig. 1a, similar to Alloy A in the same temper. The grain boundary precipitates were elemental Si and a MgSi-type phase, probably the β -phase (Mg_2Si) or a precursor, while the Cu-containing Q-phase or a precursor was also present in Alloy A. The water-quenched and underaged Alloy B showed some grain boundary precipitation, which was visible by SEM, as shown in Fig. 1b, in contrast to Alloy A in this temper, which did not exhibit grain boundary precipitation visible by field-

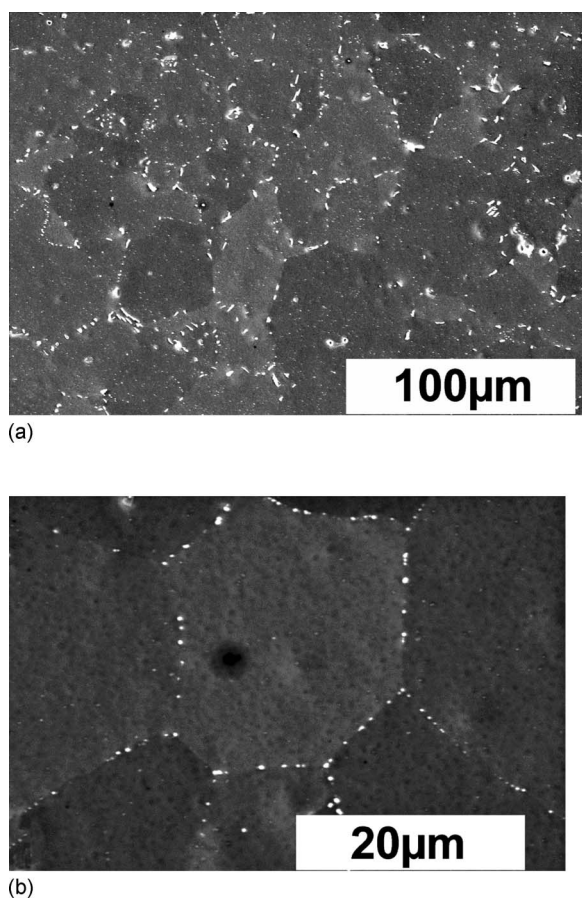


Figure 1. SEM secondary electron images of the Cu-free, unbalanced Alloy B in (a) air-cooled T4 and (b) water-quenched and underaged conditions. The samples were electropolished to enhance the contrast. Note the different magnifications of the two micrographs.

emission-scanning electron microscope.²⁸ The particles were too small for the EDS analysis by SEM. However, they were likely to be Si and MgSi-type phases.^{36,37}

The SEM investigation of fluoronitric-acid-etched samples showed that the process removed nearly all of the intermetallic particles from the surface (Fig. 2). These samples were water-cooled after homogenization and underaged. A comparison of Fig. 2a and b indicates that almost all particles were removed, leaving craters at their original locations commensurate with their sizes, except for one particle remaining on the left in Fig. 2b. Both the Fe-rich primary intermetallics and grain boundary precipitates were removed.

Analytical scanning FETEM characterization.— A scanning FETEM micrograph of a typical grain boundary area in Alloy B is shown in Fig. 3, along with EDS maps for Si, Cu, and Mg. The material was water-quenched after solution heat-treatment and then underaged. Figure 4 shows EDS linescans for Mg, Si, and Cu across the grain boundary depicted in Fig. 3.

Figures 3 and 4 show a significant depletion of Si toward the grain boundary. The magnesium distribution appeared to be uniform near the grain boundary. The EDS maps of Fig. 3 have not been normalized and therefore do not represent absolute intensities. The relatively high absolute intensity of the Mg signal in Fig. 4 was caused by partial overlap with the strong adjacent Al peak and the noise present in the signal. This was also the case for the Si signal, although to a smaller degree. Because the bulk Cu content was small (0.004 wt %), the Cu signal in Fig. 4 was at the noise level with the exception of the grain boundary, as indicated by the standard deviation

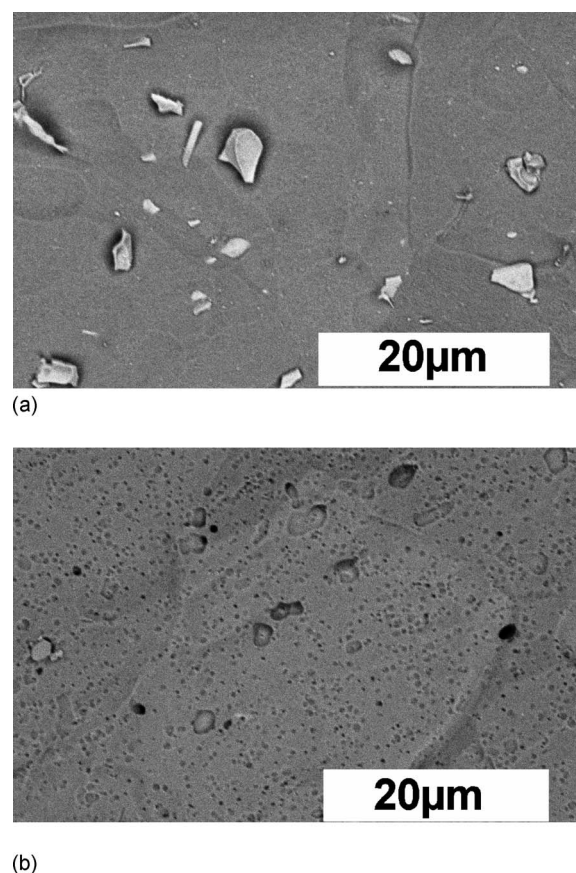


Figure 2. Back-scattered electron images of (a) an alkaline-etched and desmuted sample and (b) a sample etched for 30 s in fluoronitric acid to remove surface intermetallics (Alloy A). The sample was homogenized, water-quenched, and underaged.

of the Cu signal, which is also plotted. At the grain boundary, the Cu signal appeared to be detectable at a statistically significant level above the noise.

Similar FETEM micrograph and EDS maps of water-quenched and underaged Alloy A have been presented and discussed earlier,²⁴⁻²⁸ showing not only the similar grain boundary features as far as Si and Mg are concerned, but also the presence of a few

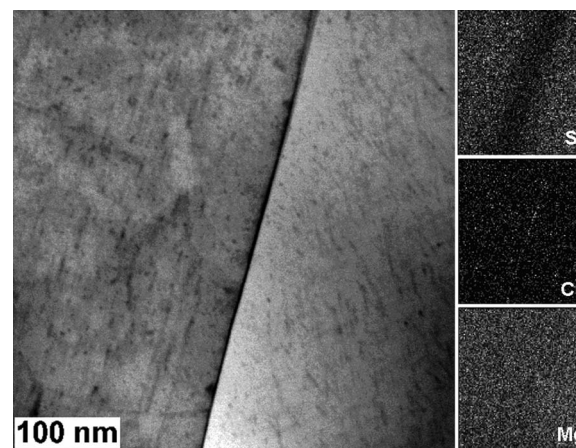


Figure 3. Scanning TEM micrograph of grain boundary region in Alloy B (water-quenched and underaged) and the corresponding EDS Si, Cu, and Mg element maps of the same area.

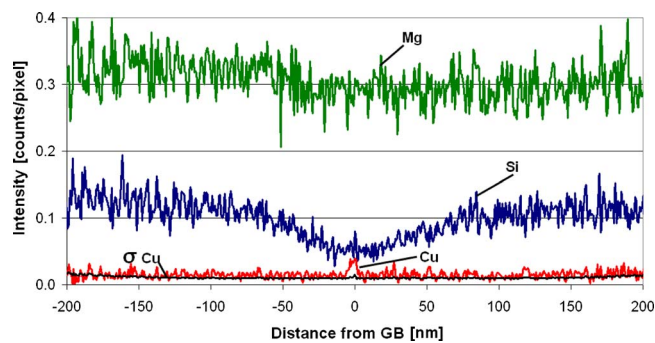


Figure 4. (Color online) Element composition profiles across a grain boundary in Alloy B (water-quenched and underaged). The profiles were extracted from the maps shown in Fig. 3 by using the analysis method discussed in Ref. 28.

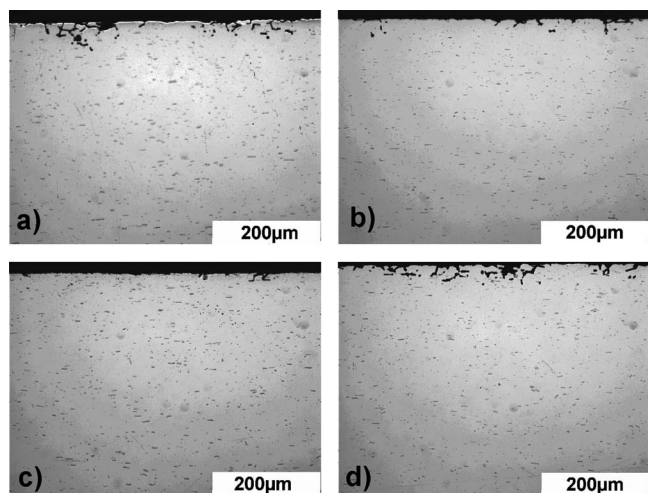


Figure 5. Cross-sectional micrographs of air-cooled variants of alloy B after corrosion test: (a) Naturally aged (T4), (b) underaged (42 min at 185°C), (c) peak-aged (T6), and (d) overaged (24 h at 185°C).

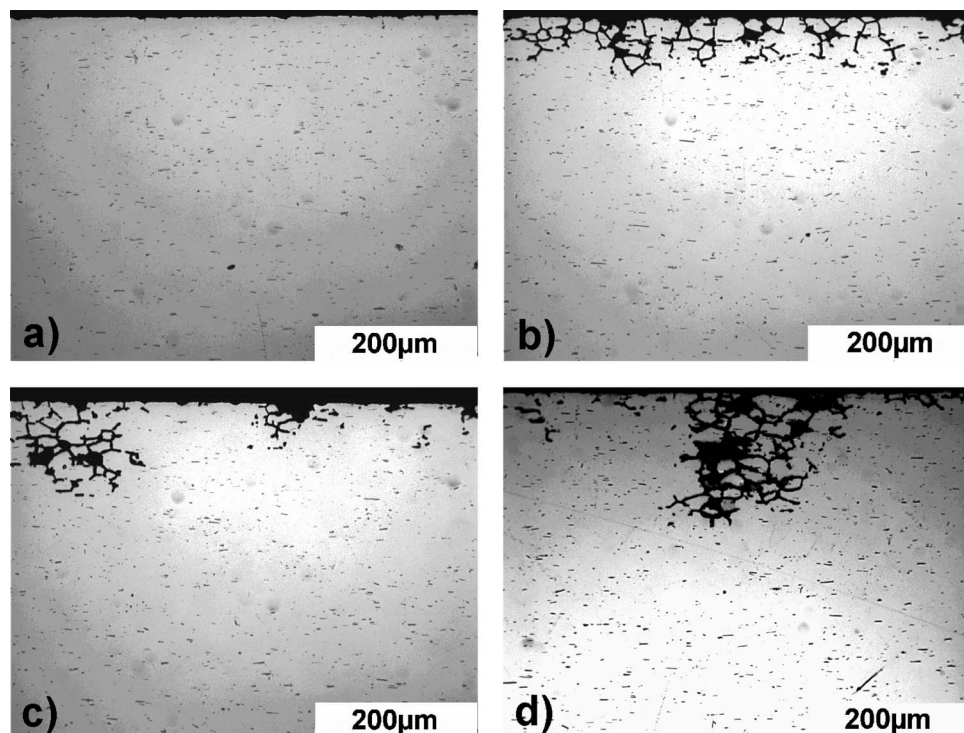


Figure 6. Cross-sectional micrographs of water-quenched variants of Alloy B after corrosion test. (a) Naturally aged (T4), (b) underaged (42 min at 185°C), (c) peak-aged (T6), and (d) overaged (24 h at 185°C).

nanometer thick, continuous Cu-rich film along the grain boundary, giving a sharp, high intensity peak in the linescan at the grain boundary.²⁸ Structure of the film could not be determined because of its small thickness and instrumental limitations. However, the segregation of such Cu-rich, continuous grain boundary films was concluded to be a common feature of the underaged temper of Cu-containing 6000-series alloys investigated in our work.

Accelerated corrosion testing.—The corrosion performance of alloys similar to Alloy A has been studied in detail using both the present accelerated test²⁴⁻²⁸ and long-term atmospheric exposure to marine environment.²⁴ In summary, the alloys were highly susceptible to IGC when they were slowly cooled after extrusion or solution heat-treatment. Artificial aging reduced the susceptibility with increasing aging toward the peak strength T6 condition. Samples, which were rapidly quenched in water after high temperature heat-treatment, showed high IGC susceptibility after aging to an underaged temper that was reduced after further artificial aging.

Metallographic cross sections of corrosion tested variants of Alloy B are shown in Fig. 5 and 6. The air-cooled T4 samples were only slightly susceptible with very superficial intergranular attack, despite the extensive grain boundary precipitation seen in Fig. 1a. No significant differences in corrosion susceptibility could be observed between the different tempers shown in Fig. 5. The water-quenched material was highly resistant to corrosion in the T4 temper, as shown in Fig. 6a. In the underaged temper, the material showed uniform IGC, but to a very shallow depth (Fig. 6b). In the peak-aged (Fig. 6c) and overaged (Fig. 6d) tempers, IGC attack was less but more localized and sparsely distributed on the surface. However, individual attack sites were deeper than for the underaged condition, reaching a maximum depth of approximately 250 µm. IGC of Cu-free, excess Si Alloy B was thus observed to repassivate after a certain depth was reached, while the Cu-containing alloy still continued to corrode at the end of the 24 h test period, with the depth of attack reaching more than 500 µm for the susceptible underaged temper.

Figure 7a and b shows cross-sectional IGC morphology of Alloys A and B, respectively. Both alloys were homogenized, water-quenched, and treated to the underaged temper. These samples were etched in a NaOH solution and desmutted in nitric acid, as described

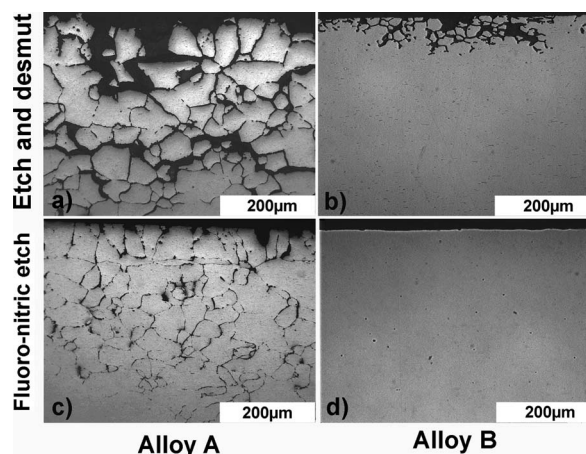


Figure 7. Cross-sectional micrographs of corrosion-tested samples. (a) Alloy A and (b) B, respectively, alkaline-etched followed by desmutting in HNO_3 . [(c) and (d)] The same materials etched in fluoronitric acid to remove surface intermetallics. Both alloys were homogenized, water-quenched, and treated to the underaged temper.

above, before subjecting to the accelerated IGC test. Both alloys showed IGC attack on the entire exposed sample surface in the underaged condition. However, the depth of attack was much larger on Alloy A than on Alloy B. Figure 7c and d shows the corresponding results for Alloy A and Alloy B after the samples were etched in fluoronitric acid to remove the intermetallic particles before the corrosion test. Alloy A still suffered deep and extensive IGC, although the width of the IGC filaments was smaller than the test sample etched in NaOH, as shown in Fig. 7c. The Cu lean unbalanced alloy (Alloy B) became completely resistant to corrosion as a result of the fluoronitric acid etch treatment (Fig. 7d). Although not shown here, results similar to Fig. 7c and d were obtained on samples, which were etched in NaOH and desmuted (intermetallics not removed) and then exposed to IGC test solution, from which oxygen was removed by nitrogen bubbling. Removal of oxygen from the solution and particles from the sample surface thus resulted in the same type of corrosion behavior by reducing the effect of the external cathodes on the IGC process.

Table III gives a summary of grain boundary microstructure and corrosion test results for all tempers of Alloys A and B.

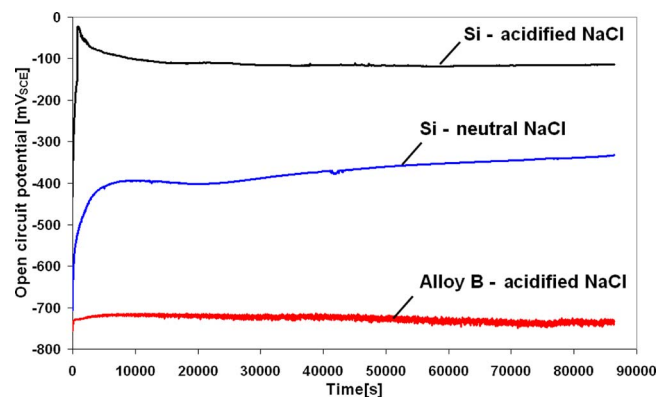


Figure 8. (Color online) Corrosion potential of elemental Si in neutral and acidified (1 vol % HCl) NaCl solutions. Corrosion potential of Alloy B in acidified NaCl solution is included for comparison. Alloy B sample was air-cooled after homogenization and naturally aged (T4).

Electrochemical measurements.— Open-circuit potential time measurements obtained in chloride solutions (Fig. 8) suggested that Si was highly cathodic (noble) compared to the aluminum Alloy B (air-cooled T4). In acidic chloride solution, the potential difference between Si and the base metal was in the range of 500–600 mV.

Pure Si electrodes were potentiostatically polarized at $-750 \text{ mV}_{\text{SCE}}$ in the same solutions as above, and the corresponding current density time data were recorded, as shown in Fig. 9. The applied potential of $-750 \text{ mV}_{\text{SCE}}$ was selected because it corresponds to the typical corrosion potential of commercially pure and moderately alloyed aluminum alloys in chloride media at 25°C . Potentiodynamic polarization testing was also performed in the negative potential direction, starting from the initial corrosion potential, in the acidified chloride solution, as shown in Fig. 10. A polarization curve for copper, obtained under identical conditions, is also included for comparison. The cathodic current levels measured in these experiments for silicon were, in general, very small. The cathodic current density of silicon was much smaller than that of copper in the potentiodynamic experiment (Fig. 10). These results show that Si is an electrokinetically poor cathode in both neutral and acidified solutions, although the corrosion potential data may suggest the opposite.

Table III. Overall summary of results.

Alloy	Temper	Corrosion type	Grain boundary precipitates	Grain boundary depletion	Reference	
A	Water-cooled T4	Superficially etched; no IGC	ND; slight Si and Cu enrichment	ND	28, 29, and TW	
	Underaged	Extensive IGC	Q' dispersoids connected with continuous Cu film	Si and slight Mg	28 and 29	
	T6	Slight, localized IGC	Discrete Q-phase particles	ND	28 and 29	
	Overaged	Slight, localized IGC	Discrete Q-phase particles	ND	28 and 29	
	Air-cooled T4	Extensive IGC	Q' dispersoids connected with continuous Cu film	ND	24–27 and 29	
	Underaged	Extensive IGC	Q' dispersoids connected with continuous Cu film	NC	24–27 and 29	
	T6	Slight, localized IGC	Discrete Q-phase particles	ND	24–27 and 29	
	Overaged	Slight, localized IGC	Discrete Q-phase particles	ND	24–27 and 29	
	B	Water-cooled T4	No IGC	Si and MgSi precipitates	ND	TW
		Underaged	Shallow IGC	Si and MgSi precipitates	Si	TW
T6		Shallow, localized IGC	Si and MgSi precipitates	ND	TW	
Overaged		Shallow, localized IGC	Si and MgSi precipitates	ND	TW	
Air-cooled T4		Slight IGC	Si and MgSi precipitates	NC	TW	
Underaged		Slight IGC	Si and MgSi precipitates	Si	TW	
T6		Slight IGC	Si and MgSi precipitates	ND	TW	
Overaged		Slight IGC	Si and MgSi precipitates	ND	TW	

ND: Not detectable, NC: Not characterized, and TW: This work.

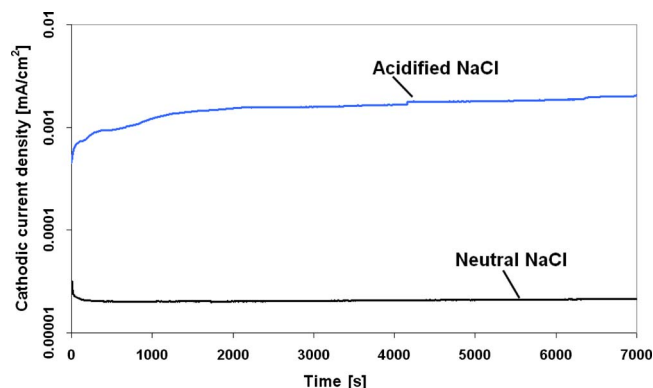


Figure 9. (Color online) Cathodic current density due to potentiostatic polarization of elemental Si at -750 mV_{SCE} in neutral and acidified 3% NaCl solutions exposed to ambient atmosphere.

Discussion

An important conclusion of this paper is that the presence of a small amount of copper in Alloy A (0.18 wt % Cu and 0.6 wt % Si) is much more effective than excess silicon in Alloy B (0.008 wt % Cu and 1.3 wt % Si) for promoting IGC susceptibility. As both alloys exhibit solute-depleted zones along the grain boundary in the susceptible tempers, this contributes to IGC susceptibility. The main difference between the two alloys is the type and location of the cathodic sites. Although the grain boundaries are decorated with the continuous Cu-rich film as the in situ cathode for the susceptible tempers of Alloy A (Cu-rich), the Fe-rich primary phases on the surface are the only cathodes available in Alloy B (Cu-free, excess Si). Elemental Si precipitates, which are present along the grain boundaries of Alloy B, have often been suggested to be cathodic to the aluminum matrix.^{5,7,8,13,14,38} The present data support other studies¹⁵⁻¹⁷ suggesting that Si is an inefficient cathode. The effectiveness of phases as cathodes cannot be judged based solely on corrosion potential measurements, especially if the surface of the material is passive. Electrochemical polarization data have to be obtained and considered.

In the presence of Cu-rich film along the grain boundary, the cathode is present where the corrosion occurs. In the external cathodes, the rate and extent of IGC are governed by the ohmic potential drop. The ohmic resistance in the solution becomes very large in a cavity of nanometer thickness near the tip of a growing IGC filament. Repassivation of IGC after the filaments reach a certain length can thus be explained, while widening of the filaments can continue to occur. Conversely, in the presence of the Cu-rich film acting as

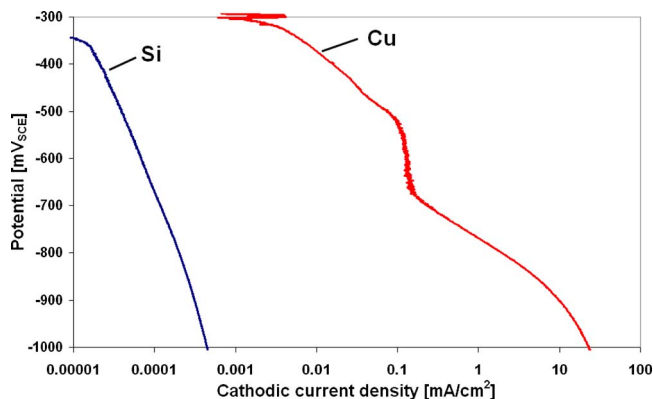


Figure 10. (Color online) Cathodic polarization curve of elemental Si in acidified NaCl solution. Scan rate was 6 mV/min. The cathodic polarization curve of elemental Cu is included for comparison.

the cathode along the path of IGC filament, propagation of narrow filaments to much larger depths can be justified. However, the effect of the internal cathode is significantly reduced as a result of transformation of the film into discrete particles by artificial aging, as discussed in an earlier paper.²³ The absence of a continuous Cu-rich film in this case significantly reduces the driving force for IGC from one Q-phase particle to the next, i.e., the presence of solute-depleted zones and discrete particulate cathodes is not sufficient in promoting IGC in the investigated alloy. The IGC resistance obtained for Alloy B by the removal of the external cathodes or purging the dissolved oxygen from the solution and the persisting susceptibility of under-aged Alloy A after the same treatment are good evidence for the fact that the continuous-film internal cathode in an AlMgSi alloy is a much more effective IGC promoter than the external cathodes, discrete internal cathodes, and the solute-depleted zone alone. The presence of the solute-depleted zone together with a continuous-film cathode segregated along the grain boundary is the optimal condition for rapid IGC.

An interesting observation, obtained from the particle removal experiment, is that the width of IGC filaments in Alloy A was appreciably reduced, although the depth of attack was unchanged. From a practical viewpoint, the expected damage imparted to a bearing structure would be unchanged. However, this result shows that the external cathodes clearly contribute to IGC, although this contribution appears to be restricted to filament widening. In situ observation of IGC propagation by X-ray tomography experiments,³⁹ which were limited to the observation of the widening phase of the IGC filaments because of the spatial resolution of the method, showed that the widening occurred at a constant volume rate. This implies, in essence, that the corrosion occurred at a constant rate of weight loss. A possible explanation is that the available cathode area and the rate of cathodic reaction per area were constant when the filament widening occurred, and this behavior can be attributed to the external and internal cathodes at a constant area as the driving force. The Cu film may lose efficiency as a cathode during filament widening because it may be destroyed by IGC propagation. It may also redeposit on the grain walls as indicated in an earlier analysis,²⁶ contributing to the total cathode area during the filament widening phase. The ohmic potential drop is also expected to be smaller for filament widening with the external cathodes as the driving force because the ohmic resistance in the filaments is expected to become smaller by reduction in the geometrical constriction, and the current density on the filament wall becomes much smaller in relation to the expected high current density at the filament tip. The external cathodes must also be important in contributing to the initiation of IGC.

The evidence supporting the significance of Cu-rich grain boundary film in the Cu-containing Alloy A compared to the external cathodes in causing susceptibility to IGC can be summarized stepwise as follows:

1. Cu-free Alloy B, with external cathodes or oxygen in the bulk solution removed, shows no IGC even though Si-rich particles may be present on the grain boundaries.
2. Si-rich particles are not good cathodes.
3. External cathodes are required to cause IGC on Alloy B.
4. External cathodes are still not as effective as the internal Cu-rich film along the grain boundaries of Alloy A to cause deep penetrating IGC. IGC caused by internal cathodes on Alloy B is insignificant compared to IGC on Alloy A.
5. Cu-containing Alloy A, with the external cathodes or oxygen in the bulk removed, still shows deep penetrating IGC.
6. Equivalent of Alloy A, containing even a smaller amount of Cu (0.02 wt %), did not show any IGC.²⁸
7. One of the reasons why external cathodes do not cause significant IGC is the ohmic potential developing with increasing depth of IGC attack. Because of the presence of Cu-rich film along the grain boundary of Alloy A, ohmic potential drop is a smaller limitation for the development of deep IGC attacks.

Localized corrosion of aluminum alloys, driven by internal cathodes alone, is a special phenomenon in practice because the external cathodes are required for acidification of the localized anolyte. In the absence of the external cathode, the localized anolyte may not become acidified because the oxidation, along with hydrolysis (pH-reducing), and reduction (pH-increasing) reactions occurring inside the filament may neutralize the anolyte. An important exception is the filiform corrosion. However, acidified anolyte must be available, in this case, at the outset of filament propagation, e.g., as a result of pitting corrosion before the onset of the filiform filament propagation.⁴⁰ The small volume of acidified electrolyte produced in the pit then follows the filament head to satisfy the electroneutrality condition there. In the IGC propagation in this work, it can be argued that the acidity of the filament tip is maintained because the specimens are immersed in an acidified chloride test solution. The external cathodes, albeit of smaller significance in the present study, may also contribute to maintaining the acid anolyte. However, we have shown earlier that the Cu-containing alloys similar to Alloy A in the underaged condition are more susceptible to IGC than their aged counterparts in field tests conducted in neutral marine atmosphere to validate the use of the accelerated test for our present purpose.²⁴

We have presented evidence about the significance of copper in causing IGC corrosion of underaged AlMgSi alloys in our earlier work.²⁴⁻²⁸ The present study has provided additional evidence indirectly supporting the earlier conclusions by showing the relative insignificance of excess Si alone in causing IGC of 6000-series alloys, which has been regarded in the past as an important cause of IGC of commercial 6000-series alloys, as reviewed earlier in this paper. The evidence provided in the present and earlier papers show the importance of Cu in relation to excess Si in the underaged condition. Because 6000-series alloys are aged to peak strength T6 temper in most applications, which is also shown by this work to be a relatively IGC-resistant temper for these alloys, the IGC problem due to Cu has not been discussed much in the literature. The presence of Cu even in as small concentrations as 0.1% has to be carefully considered in evaluating IGC susceptibility of 6000-series alloys, as indicated by Hug nearly 70 years ago.¹

Another significance of the present results is in showing the importance of internal cathodes in relation to external cathodes in localized corrosion, although the results are specific to IGC. Several questions, especially with regard to maintenance of acid conditions in the anolyte by internal cathodes, can be answered by obtaining better information about the nature of solution chemistry in localized corrosion, which is not adequate at present.

Conclusions

1. Two model alloys, one Cu-containing and one Cu-free with a large excess of Si, have been heat-treated to similar tempers and tested under similar conditions. According to the accelerated test method used, the Cu-containing alloy was significantly more susceptible to IGC than the Cu-free alloy in terms of both the extent of attack and depth of penetration.

2. The tendency of the Cu-free alloy with Si excess to IGC was superficial in comparison after exposure to the accelerated test. Therefore, the IGC susceptibility of the alloy would be insignificant under the most practical exposure conditions.

3. The Cu-containing alloy was susceptible to IGC especially in the underaged condition. Aging to the peak strength T6 reduced the susceptibility.

4. Although aging slightly increased IGC on the Cu-free alloy with excess Si, corrosion behavior of this alloy was relatively independent of temper.

5. The greater susceptibility of the Cu-containing underaged alloy to IGC was caused by a continuous Cu-rich nanofilm segregated along the grain boundaries as the internal cathode, together with a solute-depleted active zone adjacent to the grain boundary. Trans-

forming of the film by further aging reduced the susceptibility to IGC.

6. The depth of IGC attack in the susceptible Cu-containing alloy was primarily determined by the internal Cu-rich film cathode. The material was susceptible to IGC even in the absence of external cathodes. The external cathodes contributed to filament widening. The external cathodes were primarily the Fe-rich intermetallic phases at the surface.

7. External cathodes were the driving force for any IGC occurring on the Cu-free, excess Si alloy. Elemental Si particles present along the grain boundaries did not constitute effective cathodes. The presence of a Si-depleted zone adjacent to the grain boundary contributed to IGC susceptibility.

Acknowledgments

The authors are grateful to Alison Davenport for providing useful discussion and Ragnvald Mathiesen for assistance in analyzing the EDS element maps. This work was part of a Norwegian national research program entitled "Light Metal Surface Science," supported by The Norwegian Research Council and Hydro Aluminum.

Norwegian University of Science and Technology assisted in meeting the publication costs of this article.

References

- H. Hug, *Aluminum*, **23**, 33 (1941).
- W. K. Johnson and T. E. Wright, *Aluminum*, **43**, 490 (1967).
- K. Yamaguchi and K. Tohma, *J. Japan Inst. Met.*, **47**, 285 (1997).
- K. Yamaguchi and K. Tohma, in *Proceedings of the 6th International Conference on Aluminium Alloys*, T. Sato, S. Kumai, T. Kobayashi, and M. Murakami, Editors, Japan Institute of Light Metals, p. 1657 (1998).
- Aluminium—Properties and Physical Metallurgy*, J. E. Hatch, Editor, American Society for Metals International, Metals Park, Ohio (1984).
- R. Dif, D. Bechet, T. Warner, and H. Ribes, in *Proceedings of the 6th International Conference on Aluminium Alloys*, T. Sato, S. Kumai, T. Kobayashi, and M. Murakami, Editors, Japan Institute of Light Metals, p. 1991 (1998).
- R. Steigerwald, *Metals Handbook*, Vol. 13, 9th ed., p. 123, American Society for Metals International, Metals Park, Ohio (1987).
- A. K. Bhattamishra and K. Lal, *Z. Metallkd.*, **89**, 793 (1998).
- T. D. Burleigh, E. Ludwiczak, and R. A. Petri, *Corrosion (Houston)*, **51**, 50 (1995).
- V. Guillaumin and G. Mankowski, in *Proceedings of Critical Factors in Localized Corrosion III*, R. G. Kelly and G. S. Frankel, Editors, PV 98-17, p. 203, The Electrochemical Society, Pennington, NJ (1999).
- V. Guillaumin and G. Mankowski, *Corros. Sci.*, **42**, 105 (2000).
- V. S. Sinyavskii, V. V. Ulanova, and V. D. Kalinin, *Prot. Met.*, **40**, 481 (2004).
- A. Shi, B. A. Shaw, and E. Sikora, *Corrosion (Houston)*, **61**, 534 (2005).
- D. O. Sprowls and R. H. Brown, in *Proceedings of Fundamental Aspects of Stress Corrosion Cracking*, The Ohio State University, p. 466 (1967).
- O. Lunder and K. Nisancioglu, in *Progress in the Understanding and Prevention of Corrosion*, Vol. 2, J. M. Costa and A. D. Mercer, Editors, p. 1249, The Institute of Materials, London (1993).
- K. Mizuno, A. Nylund, and I. Olefjord, *Corros. Sci.*, **43**, 381 (2001).
- F. Sertcelik, A. F. Cakir, M. Ürgen, D. Gabe, and D. Ross, in *Proceedings of the European Corrosion Congress EUROCORR*, European Federation of Corrosion, p. 297 (1997).
- L. F. Mondolfo, *Aluminium Alloys: Structure and Properties*, Butterworths, London (1976).
- L. F. Mondolfo, *Manganese in Aluminium Alloys*, Page Bros, Norwich, U.K. (1977).
- A. K. Bhattamishra and K. Lal, *Mater. Des.*, **18**, 25 (1997).
- R. Chadwick, N. B. Muir, and H. B. Grainger, *J. Inst. Met.*, **82**, 75 (1953).
- M. Zamin, *Corrosion (Houston)*, **37**, 627 (1981).
- H. Uchida, H. Yoshida, H. Hira, and T. Amano, *Mater. Sci. Forum*, **217-222**, 1753 (1996).
- G. Svenningsen, J. E. Lein, A. Bjørgum, J. H. Nordlien, Y. Yu, and K. Nisancioglu, *Corros. Sci.*, **48**, 226 (2006).
- G. Svenningsen, M. H. Larsen, J. C. Walmsley, J. H. Nordlien, and K. Nisancioglu, *Corros. Sci.*, **48**, 1528 (2006).
- G. Svenningsen, M. H. Larsen, J. H. Nordlien, and K. Nisancioglu, *Corros. Sci.*, **48**, 258 (2006).
- G. Svenningsen, M. H. Larsen, J. H. Nordlien, and K. Nisancioglu, *Corros. Sci.*, **48**, 3969 (2006).
- M. H. Larsen, J. C. Walmsley, O. Lunder, R. H. Mathiesen, and K. Nisancioglu, *J. Electrochem. Soc.*, **155**, C550 (2008).
- M. H. Larsen, Ph.D. Thesis, Norwegian University of Science and Technology, Trondheim, Norway, In progress.
- H. Leth-Olsen and K. Nisancioglu, *Corros. Sci.*, **40**, 1179 (1998).
- H. Leth-Olsen, A. Afseth, and K. Nisancioglu, *Corros. Sci.*, **40**, 1195 (1998).
- H. Leth-Olsen, J. H. Nordlien, and K. Nisancioglu, *Corros. Sci.*, **40**, 2051 (1998).

33. P. Campestri, E. P. M. van Westing, and J. H. W. de Wit, *Electrochim. Acta*, **46**, 2553 (2001).
34. O. Lunder, K. F. Heen, and K. Nisancioglu, *Corrosion*, **60**, 622 (2004).
35. British Standard BS 11846 (1995).
36. D. G. Eskin, *J. Mater. Sci.*, **38**, 279 (2003).
37. D. G. Eskin, V. Massardier, and P. Merle, *J. Mater. Sci.*, **34**, 811 (1999).
38. F. Andreatta, A. Turco, I. de Graeve, H. Terryn, J. H. W. de Wit, and L. Fedrizzi, *Surf. Coat. Technol.*, **201**, 7668 (2007).
39. M. H. Larsen, J. Mårdalen, A. J. Davenport, F. Eckermann, F. De Carlo, and K. Nisancioglu, in *Proceedings of 14th Nordic Corrosion Congress*, Technical University of Denmark, p. 13–15 (2007).
40. R. T. Ruggeri and T. R. Beck, *Corrosion*, **39**, 452 (1983).